

Binuclear $s = 1/2$ single molecular magnets with the symmetry restrictions

A. V. Zhuravlev

*Donetsk Institute for Physics and Engineering named after O. O. Galkin, National Academy of Sciences of Ukraine
Kyiv 03028, Ukraine*

E-mail: alexander.zhuravlev01@gmail.com
cranealex1@gmail.com

Received July 1, 2021, published online September 24, 2021

Exchange anisotropy effects in equal-spin $s^{(1)} = s^{(2)}$ dimeric single-molecule magnets exhibiting C_2 point-group symmetry have been studied. The Hamiltonian, which is written in two-spin 4×4 Pauli matrixes representation in the appropriate noncollinear local coordinates systems, has been transformed to common coordinates and used to derive energy levels and spin eigenstates. An anomalous variation of the magnetic system average spin depending on the misalignment of the local anisotropy axes has been found. Particularly, a fully nonmagnetic state of an $s = 1/2$ spin dimer and “silent” EPR mode has been predicted. The angular boundaries of the EPR existence have been determined for any possible mutual deflections of the local ion axes for each of the 6 possible transitions between the levels of the spin system, both in zero and in a nonzero magnetic field.

Keywords: molecular magnetism, exchange interactions (electron), magnetic anisotropy, spin crossover, EPR spectroscopy.

1. Introduction

Polynuclear metal complexes make a series of new molecular magnetic systems [1] with unusual physical properties due to their potential uses in magnetic storage and quantum computing [1]. Since the paramagnetic ions in a single molecular magnet (SMM) are surrounded by extended nonmagnetic ligands, we can neglect the intermolecular magnetic interactions and merely use intramolecular ones. Then an SMM can be described with a Hamiltonian of a system of N spins s . The local surrounding of paramagnetic ions in SMM, which forms tetrahedral or octahedral bricks, is usually equal but their orientation may vary with substantial angles between their local axes. Therefore, it is necessary to consider the local symmetry of the crystal field of each magnetic ion and the global symmetry of SMM.

There are many systematic theoretical approaches considering the symmetry of SMM that is based on the irreducible tensor operator technique [2] and its extension considering the permutation symmetry [3], on the algebraic combinatorics [4], or present point-group and shift operator technique [5]. None of them considers energy spectra and spin state variation with local crystal ion field axis divergence.

Despite the essential progress of the numerical analysis simulation techniques and the computer capabilities in in-

vestigating Hamiltonians of spin systems of a wide range of SMM, the realistic arrangements of the local anisotropy tensors make problems with calculations and require studying the simplest spin system. The simplest are binuclear SMM, or spin (magnetic) dimers V^{4+} or Cu^{2+} with an $s = 1/2$ spin.

The magnetic properties of the binuclear complexes V^{4+} , $VO(HPO_4) \cdot 0.5H_2O$, and $KZn(H_2O)(VO)_2(PO_4)_2(H_2PO_4)$ reflect strong spin-spin correlations [6]. A remarkable feature of both of these vanadophosphates is the ligand arrangement with V^{4+} ions placed inside face-sharing VO_6 octahedra. The resulting vanadium dimer, V_2O_9 , has some misalignment between neighboring octahedral axes for an angle about $\pi/2$ with an approximate C_2 symmetry.

A number of binuclear Cu^{2+} complexes has been synthesized and studied up to now [7–40], which can be divided into six groups only by the type of molecular symmetry. The Cu^{2+} dimers with long bridging ligands are out of our interest because a weak Cu–Cu exchange interaction destroys the cooperative magnetic effects of the Cu^{2+} cluster. In addition, not all of the known Cu_2 compounds have been studied in detail to get an unambiguous idea of the local environment of Cu^{2+} .

The copper complex of salicylidenehydrason glutarin acid (H_4L) $[Cu_2L_2(Py)_2MeOH]$ has a close-to-flat ionic environment. Ligand planes of Cu_2 have rotated relatively $Cu^{(1)}$

ligand about $\pi/2$ around Cu–Cu link direction [7]. This rotation can be represented with all 3 Euler angle rotations about $\pi/2$. Ligands belonging to Cu⁽¹⁾ and Cu⁽²⁾ in [Cu₂L₄Py], where H₄L is adipoilhydrason of 2-hydroxipropiophenon rotated about π angle around Cu–Cu link [7]. [Cu₂(pAB)₂(phen)₂pz] (pABH = p-aminobenzoic acid, phen = 1,10-phenanthroline, and pz = pyrazine) has square pyramidal surrounding of Cu ions obeying the C₂ symmetry [8]. The axial axes of Cu⁽¹⁾ and Cu⁽²⁾ surrounding pyramids are misaligned about an angle close to π .

With identical ligands making up the complex, the mutual orientation of the local coordinate systems (LCS) can be determined from the orientation of the pyramids, octahedra, or squares of the nearest environment of paramagnetic ions. The axial axes of the ligands and the direction of the bond between the spins are further taken as the z axes of the local coordinate system and as the x axis, respectively. Most Cu₂ SMM with strong ion bonds have high molecular symmetry in which the axial LCS axes coincide. Only a few compounds have significant LCS z -axis deflections.

The object of interest is the effects caused by the deflection of the axes of local anisotropy from the axis of the molecular coordinate system (MCS). The close environment of copper ions usually has a high symmetry and coinciding z axes of the ligands. Quite few compounds have misaligned LCS z axes.

To study the response of the SMM magnetic system to the noncollinearity of the local anisotropy axes, a spin symmetry analysis model has been developed in the representation of local coordinate systems of individual spins using Pauli matrices. The effect of symmetry on the energy spectra, spin states, and EPR spectra of the $s = 1/2$ dimer has been considered in detail for the operation C₂¹ rotation about MCS z axis at π . The results of applying other symmetry operations to the spin dimer are quite obvious and discussed in Sec. 4.

2. $s = 1/2$ dimer theoretical model

The presented microscopic model describes the interaction of local spins and contains terms corresponding to the isotropic exchange interaction (\hat{H}_{is}), axial and rhombic (azimuthal) anisotropy (\hat{H}_{ax} , \hat{H}_{rh}), and the interaction of spins with a magnetic field (\hat{H}_{Zeem}):

$$\hat{H} = \hat{H}_{is} + \hat{H}_{ax} + \hat{H}_{rh} + \hat{H}_{Zeem} . \quad (1)$$

For a magnetic system of two $s = 1/2$ spins, the basic observables are the spin operators of each site in the LCS representation

$$\tilde{s}^{(1)} = s\boldsymbol{\sigma} \otimes \mathbf{I}, \quad \tilde{s}^{(2)} = s\mathbf{I} \otimes \boldsymbol{\sigma}, \quad (2)$$

where \mathbf{I} is the 2×2 identity matrix, $s = 1/2$, and $\boldsymbol{\sigma}$ is the Pauli spin matrices with components

$$\sigma_x = \begin{pmatrix} 0 & 1 \\ 1 & 0 \end{pmatrix}, \quad \sigma_y = \begin{pmatrix} 0 & -i \\ i & 0 \end{pmatrix}, \quad \sigma_z = \begin{pmatrix} 1 & 0 \\ 0 & -1 \end{pmatrix}. \quad (3)$$

This section assumes a situation when the orientation of the LCS axes of the 1st and 2nd ions is strictly specified by their nearest environment, i.e., the case of a crystal field that is strong in terms of the hierarchy of terms of the spin Hamiltonian. This situation is common for molecular magnets, which are, as a rule, complex metal-organic compounds. This assumption physically substantiates the local coordinate systems rather than the MCS. The former represents the spin components as follows (3).

The deflection of the MCS axes (\mathbf{x} , \mathbf{y} , \mathbf{z}) for each spin with respect to the initial, local axes ($\tilde{\mathbf{x}}^{(k)}$, $\tilde{\mathbf{y}}^{(k)}$, $\tilde{\mathbf{z}}^{(k)}$, $k = 1, 2$) is conveniently represented in the form of 3 rotations described by the Euler angles. These are: (i) rotation about $\tilde{\mathbf{z}}^{(k)}$ at φ_k , (ii) rotation about the rotated (secondary) axis $\tilde{\mathbf{y}}^{(k)}$ at θ_k , (iii) rotation about the secondary axis $\tilde{\mathbf{z}}^{(k)}$ at ψ_k .

To get “molecular” representation of the spin (2) instead of the Hamiltonian (1) in LCS, we apply to each spin rotational operators

$$U^{(k)}(\varphi_k, \theta_k, \psi_k) = U(\varphi_k)U(\theta_k)U(\psi_k) = e^{-is\sigma_z\varphi_k} e^{-is\sigma_y\theta_k} e^{-is\sigma_z\psi_k}. \quad (4)$$

Considering (2), (3), and (4), we have an equation based on the spin symmetry equivalence $\mathbf{s}^{(2)} = O \mathbf{s}^{(1)} O'$:

$$U^{(2)} \tilde{s}^{(2)} U'^{(2)} = T O U^{(1)} \tilde{s}^{(1)} U'^{(1)} O' T', \quad (5)$$

where T is a permutation operator, O is an operator of some symmetry operation, U' , T' , and O' are the transposed operators. 4×4 matrix equations (5) represent 16 equations for each of the Cartesian components of the spins, which define the relationship between the angles φ_1 , θ_1 , ψ_1 , and φ_2 , θ_2 , ψ_2 . By eliminating trivial conditions from (5), we get symmetry constraints for each of the operations of a given molecular symmetry group.

Based on the above assumptions, the paper is referring to molecular symmetry rather than crystallographic one. It should also be noted that $U^{(k)}$ in (5) have the meaning of coordinate transformation operators (“passive” interpretation of Euler’s catch), as the LCS orientation is physically fixed by a “strong” crystal field.

Let us consider a two-spin system obeying the C₂ symmetry. The rotation axis for the operation must be perpendicular to the $\mathbf{s}^{(1)}$ – $\mathbf{s}^{(2)}$ link, as only spin permutating operations can impose restrictions on the system. Equations (5), assuming the equivalence of $\mathbf{s}^{(1)}$ and $\mathbf{s}^{(2)}$ during the operation, provide the relations between the Euler angles:

$$\begin{aligned} \theta_2 &= \xi\theta_1, \\ \varphi_2 &= \varphi_1 + \pi/2 - \xi\pi/2, \\ \psi_2 &= \psi_1 + \pi/2 + \xi\pi/2, \\ \xi &= \pm 1. \end{aligned} \quad (6)$$

Although the coincidence of the cases $\xi = +1$ and $\xi = -1$ was verified by substitution in (5), the second option is physically more transparent. Considering (6), the Hamiltonian (1) can be written in the MCS representation:

$$\hat{H} = \hat{H}_{\text{is}} + \hat{H}_{\text{ax}} + \hat{H}_{\text{rh}} + \hat{H}_{\text{Zeem}}, \quad (7)$$

$$\begin{aligned} \hat{H}_{\text{is}} &= J \hat{\mathbf{s}}^{(1)} \hat{\mathbf{s}}^{(2)}, & \hat{H}_{\text{ax}} &= A_{\text{ax}} \hat{s}_z^{(1)} \hat{s}_z^{(2)}, \\ \hat{H}_{\text{rh}} &= A_{\text{rh}} (\hat{s}_x^{(1)} \hat{s}_x^{(2)} - \hat{s}_y^{(1)} \hat{s}_y^{(2)}), & \hat{H}_{\text{Zeem}} &= \sum_{k=1}^2 \hat{\mathbf{g}}_z^{(k)} \hat{s}_z^{(k)} \mathbf{H}_{\text{loc}}^{(k)}, \quad (8) \\ \hat{\mathbf{g}}_z^{(k)} &= (\mathbf{R}^{(k)})^{-1} \hat{\mathbf{g}}_z^{(k)} \mathbf{R}^{(k)}, & \mathbf{H}_{\text{loc}}^{(k)} &= \mathbf{H}, \end{aligned}$$

where $J, A_{\text{ax}}, A_{\text{rh}}$ are the isotropic exchange, axial and rhombic (azimuthal) anisotropy constants, $\hat{\mathbf{g}}_z^{(k)}$ and $\hat{\mathbf{g}}_z^{(k)}$ are the spectroscopic splitting tensor in the MCS and LCS representations, $\mathbf{R}^{(k)}$ is the three-dimensional rotation matrix, $\mathbf{H}_{\text{loc}}^{(k)}$ is the local external field at the k th spin site, \mathbf{H} is the external magnetic field ($\mathbf{H} \parallel \mathbf{z}$). Hamiltonian (7) will be further considered in the form normalized to J , i.e., $J = 1$, and characteristics of other interactions expressed in units of J .

3. Energy spectra and spin states of dimer

The spin Hamiltonian is usually represented by default in a unified laboratory coordinate system (UCS); the eigenstates can be rendered by two multiplets — a singlet and a triplet E_t . Let us designate the eigenstates as $|0,0\rangle_{\text{UCS}}$, $|1,0\rangle_{\text{UCS}}$ and $|1,1\rangle_{\text{UCS}}$. Axial anisotropy splits the triplet into singlet $|1,0\rangle_{\text{UCS}}$ with symmetric wave function $(|1/2\rangle + |-1/2\rangle)/\sqrt{2}$ and doublet $|1,1\rangle_{\text{UCS}}$, while rhombic (azimuthal) anisotropy splits doublet into $|1,1\rangle_{\text{UCS}}$ and $|1,1\rangle'_{\text{UCS}}$. The ground state of the dimer with the antiferromagnetic exchange in this standard case is $|0,0\rangle_{\text{UCS}}$ with antisymmetric function $(|1/2\rangle - |-1/2\rangle)/\sqrt{2}$. Figure 1 shows

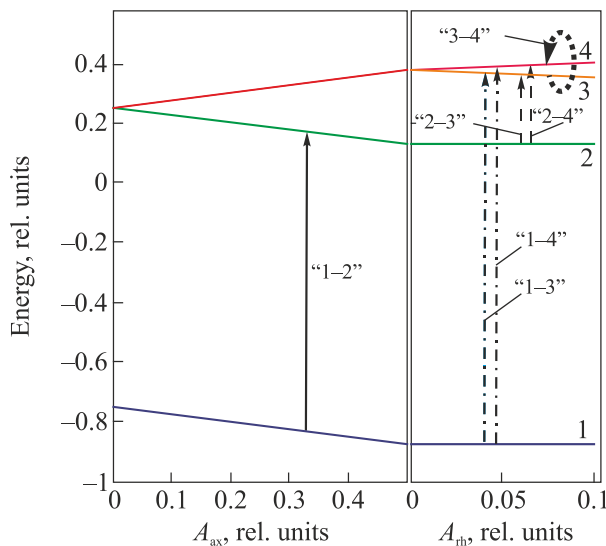


Fig. 1. (Color online) Splitting of the dimer energy spectrum with antiferromagnetic isotropic exchange interaction, the axial (A_{ax}) and rhombic anisotropy (A_{rh}). Levels are numbered near the level lines; interlevel transitions are indicated by arrows and numbers in quotation-marks.

the scheme of energy splitting by axial and rhombic anisotropy.

The $\varphi_1, \theta_1, \psi_1$ deflection of the LCS axes has practically no effect on the position of the energy levels. The singlet energy does not change at all, and the levels of the triplet experience a shift by $\sim 10^{-4}J$ when θ_1 changes from 0 to $\pi/2$.

The ground state $|0,0\rangle_{\text{UCS}}$ of the antiferromagnetic dimer of C_2 symmetry is the symmetric wave function, while the $|1,0\rangle_{\text{UCS}}$ is the antisymmetric one. The spin states of the levels were calculated as the average square values $\langle S_z^2 \rangle$ ($S_z = s_z^{(1)} + s_z^{(2)}$). The set of spin states is radically different from those existing in a system with UCS.

The deflection of the LCS axes has a strong coalescent effect on the spin states in the MCS representation. The change in the polar angle θ_1 , which directly affects the mutual orientation of the quantization axes ($\hat{\mathbf{z}}^{(k)}$), has the most significant effect. The deflection of the LCS axes in the xz plane destroys the strong exchange limit with $S_z = 0, \pm 1$ and changes the average square spins of the triplet. In the particular case $\psi_1 = 0$ and $\varphi_1 = 0$ for the deflection angle $\theta_1 = \pi/2$, the averaged spins of all states null. When the angle of rotation φ_1 of the LCS axes changes, the spin numbers of the level $|1,1\rangle'_{\text{UCS}}$ do not change, and differ significantly for

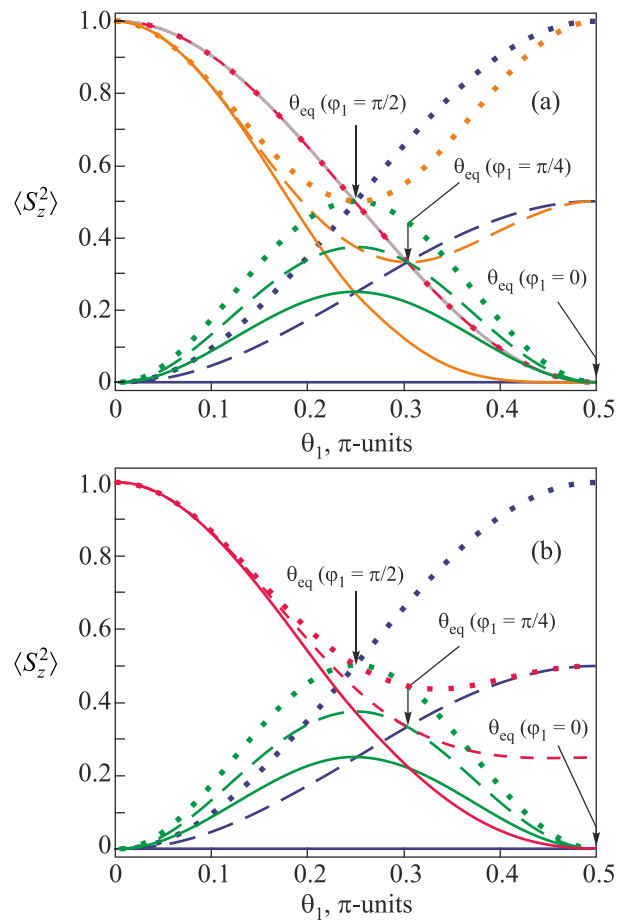


Fig. 2. (Color online) Dependences of the average square dimer spin, $\langle S_z^2 \rangle$, on the polar angle θ_1 of misorientation of the LCS axes at $\psi_1 = 0$ (a) and $\pi/4$ (b). Online color coding corresponds to Fig. 1.

other states [Fig. 2(a)]. Changes in the $\langle S_z^2 \rangle$ dimer at $\varphi_1 \neq 0$, $\psi_1 \neq 0$, and $\theta_1 \neq 0$ are quite significant and affect all states of the system (Fig. 2).

For $\varphi_1 \neq 0$, the change in the angle ψ_1 does not affect the dependence of the spin numbers of the dimer on θ_1 of the levels $|0,0\rangle_{UCS}$ and $|1,0\rangle_{UCS}$, while an increase in φ_1 leads to an increase in $\langle S_z^2(\theta_1) \rangle$, in the absence of its qualitative changes. $\langle S_z^2(\theta_1) \rangle$ of the level $|0,0\rangle_{UCS}$ grow monotonically, and show a symmetric curve with a maximum at $\theta_1 = \pi/4$ for $|1,0\rangle_{UCS}$ [Fig. 2(b)]. For $\psi_1 = \pi/4$, average spin dependences of $|1,1\rangle'_{UCS}$ and $|1,1\rangle''_{UCS}$ coincide for all φ_1 . For $\psi_1 = \pi/2$, all spin states coincide with the case $\psi_1 = 0$.

A common feature for the dependences $\langle S_z^2(\theta_1) \rangle$ for any φ_1 and ψ_1 is the existence of an “equivalence point of spin states”, θ_{eq} (Fig. 2). As φ_1 increases from 0 to $\pi/2$, the position of the “equivalence point”, shifts from $\theta_{eq} = \pi/2$ to $\theta_{eq} = \pi/4$ (indicated by a black arrow in Fig. 2). The spin numbers at the “equivalence point” increase from $\langle S_z^2 \rangle_{eq} = 0$ if $\varphi_1 = 0$ to $\langle S_z^2 \rangle_{eq} = 1/2$ if $\varphi_1 = \pi/2$.

4. EPR spectra of the dimer

4.1. Frequency-dependent EPR spectra in zero magnetic field ($\varphi_1 \neq 0, \psi_1 \neq 0, \theta_1 \neq 0, H = 0$)

The scheme of transitions between the levels of the system of a pair of interacting $s = 1/2$ spins with the C_2 symmetry differs radically from the standard EPR spectrum in the UCS representation for ac field applied along x axis. Instead of a pair of “allowed” transitions “2–3” and “2–4” ($|1,0\rangle_{UCS} - |1,1\rangle_{UCS}$) and a weak transition “3–4” ($|1,1\rangle'_{UCS} - |1,1\rangle''_{UCS}$), observed in the case $\varphi_1 = 0, \psi_1 = 0, \theta_1 = 0$ if $\varphi_1 \neq 0, \psi_1 \neq 0, \theta_1 \neq 0$, any intermultiplet transitions may be possible (Fig. 1). Since the changes in the orientation angles of the LCS do not practically affect the energy of the levels, the transition frequencies remain almost un-

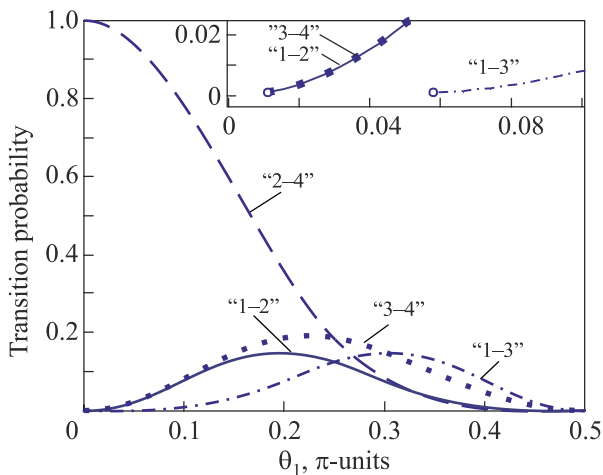


Fig. 3. (Color online) Dependences of the probability of interlevel transitions of an $s = 1/2$ dimer on the polar angle θ_1 in zero magnetic field, $\psi_1 = 0, \varphi_1 = 0$. Designations correspond to Fig. 1. The inset shows the same curve in the initial section, the points $\theta_1 = \theta_{cr}$ are marked with open circles.

changed. Nevertheless, near some values φ_1, ψ_1 and θ_1 , the intensities of certain transitions tend to zero. The minimum transition probability, which makes the EPR observation possible, turns out to be dependent on the orientation angles of the LCS. Near $\theta_1 \cong \pi/4$, up to 6 EPR lines can be ob-

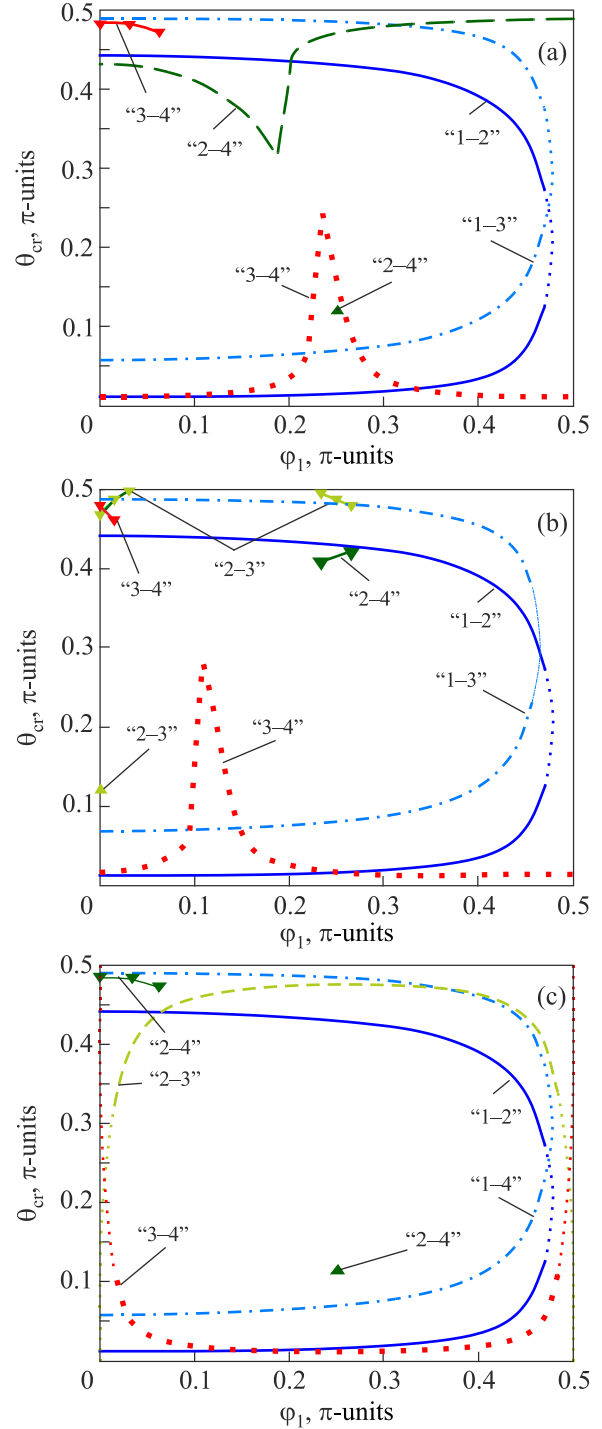


Fig. 4. (Color online) Regions of existence of the frequency-dependent EPR spectrum lines of an $s = 1/2$ dimer in zero magnetic field at different angles ψ_1 of misorientation of MCS and LCS: $\psi_1 = 0$ (a), $\pi/4$ (b), $\pi/2$ (c). Numbering and designations correspond to Fig. 1. Narrow regions of existence of EPR lines are marked with symbols \blacktriangledown for θ_{cr}^{up} and \blacktriangle for θ_{cr}^{dw} . The thin dotted line marks areas with an unsatisfactory calculation error.

served. If $\theta_1 \rightarrow 0$ or $\theta_1 \rightarrow \pi/2$, the probabilities of almost all intermultiplet transitions drop down, and when the transition $E_i - E_k$ probability decreases below the detection threshold, this EPR line disappears (Fig. 3, inset) (let us set the angle θ_1 at which $P_{ik} \cong P_{cr}$ as θ_{cr} , $P_{cr} = 10^{-3}$).

Let us denote the critical values θ_1 as θ_{cr}^{up} and θ_{cr}^{dw} for the upper and lower bounds of the EPR existence region. Figure 4 shows $\theta_{cr} - \phi_1$ diagrams with the areas of observability of each of the EPR lines.

Note that even if $\theta_1 = \phi_1 = \psi_1 = 0$, when the energy spectrum and spin states of the dimer coincide with the UCS, the EPR spectrum is different. When $\psi_1 = 0$ in the region $\phi_1 \cong 0$, there is no θ_1 angle restriction for the transitions “2–3” and “2–4”, which coincides with a dimer in UCS but exists for the “3–4” transition [Fig. 4(a)]. There is a sharp narrowing of the intervals $\theta_{cr}^{up} - \theta_{cr}^{dw}$ of the EPR line “3–4” if $\psi_1 = 0$ and $\psi_1 = \pi/4$, and the line “2–4” if $\psi_1 = \pi/4$.

There are narrow regions of signal existence near $\phi_1 \cong 0$ and $\phi_1 \cong \pi/4$ for the transitions “2–3”, “2–4”, and “3–4”. Moreover, there is a sharp increase in the signal intensity in a very narrow range of angles near some lines $\theta_{cr}^{up}(\phi_1)$ and $\theta_{cr}^{dw}(\phi_1)$ but within the EPR existence. Experimental observation in these cases will be fraught with great difficulties.

Thus, the maximum number of lines in the spectrum of the spin dimer (5–6) is in the range of $\theta_1 \sim \pi/4$, while the width of this region strongly depends on the angles ϕ_1 and ψ_1 .

4.2. $s = 1/2$ dimer spectra in nonzero magnetic field ($\phi_1 \neq 0, \theta_1 \neq 0, \psi_1 = 0, H \neq 0$)

A magnetic field, if any, along the MCS z axis transforms the magnetic system of the dimer described above. The wave functions $|1,1\rangle'_{UCS}$ and $|1,1\rangle''_{UCS}$ in the range of fields $0 - A_{rh}$ smoothly pass into $|1,-1\rangle_{UCS}$ and $|1,+1\rangle_{UCS}$. The energy of $|1,1\rangle'_{UCS}$ and $|1,1\rangle''_{UCS}$ (3 and 4, Fig. 1) nonlinearly

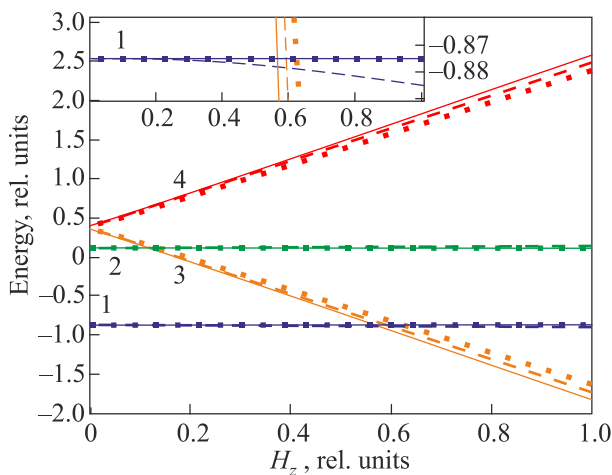


Fig. 5. (Color online) Energy spectra in a magnetic field $\mathbf{H} \parallel \mathbf{z}$ for $\theta_1 = 0$ (solid lines), $\pi/4$ (dashed lines), $\pi/2$ (bold dotted lines); $\phi_1 = 0, \psi_1 = 0$. The inset shows a scaled-up region of the level 1 spectrum. Online color coding corresponds to Fig. 1.

depend on the field in the region $H_z < A_{rh}$, the energy gap in zero field is $0.5A_{rh}$ (Fig. 5). Their shift with a change in the angle θ_1 is linear and quite obvious. The levels $|0,0\rangle_{UCS}$ and $|1,0\rangle_{UCS}$ are not affected by the magnetic field at $\theta_1 = 0$. As the field increases at $\theta_1 \neq 0$, their shift stays nonlinear, reaches a maximum at $\theta_1 = \pi/4$ (+0.01 and -0.01 at $H_z = 1$, respectively) and decreases to zero at $\theta_1 \rightarrow \pi/2$.

Figure 6 shows the EPR dimer spectra in the case $\phi_1 = 0, \psi_1 = 0, \theta_1 \neq 0$. The field dependences of the transition frequencies of the EPR from levels 1 and 2 to levels 3 and 4 are substantially nonlinear in the region $H_z < A_{rh}$. The change in the frequency-field dependences of the EPR with the deflection of the LCS axes is associated with the axial local anisotropy ($g_{zz} = 2.2, g_{xx} = g_{yy} = 2.0$) and, therefore, is very small. The intensities of the lines differ significantly with the variation of the θ_1, ϕ_1 and ψ_1 .

If $\theta_1 = 0, \phi_1 = 0, \psi_1 = 0$, there are only 2 EPR lines corresponding to the “2–3” and “2–4” transitions, probability of these transitions decreases monotonously together with θ_1 rise. The deflection of the LCS axes to the angle $\theta_1 = \pi/4$ leads to the appearance of inter- and intramultiplet transitions “1–2”, “1–3”, “1–4”, and “3–4”, their intensity increases, at least up to $\theta_1 = \pi/4$, then it decreases, and only the transition “1–2” is observed near $\theta_1 \cong \pi/2$ (Fig. 6). Lines “2–3” at $\theta_1 = 0$ and “1–4” at $\theta_1 = \pi/4$ weakens in low fields, and is not observed in $H_z < 0.002$.

If $\phi_1 = \pi/4, \psi_1 = 0$, the EPR remains present at different θ_1 for all transitions, except for “3–4”. The latter exists only in low fields, up to ~ 0.03 , at $\theta_1 = \pi/4$, and shows itself in any fields at $\theta_1 = \pi/2$. All 6 EPR dimer lines can be observed at $\theta_1 = \pi/2$.

If $\phi_1 = \pi/2, \psi_1 = 0$, only intramultiplet transitions can be observed, and “3–4” found only near $\theta_1 = \pi/4$. If $\phi_1 = \pi/2, \psi_1 = 0, \theta_1 = \pi/2$, then EPR is not observed in the dimer (“silent” mode).

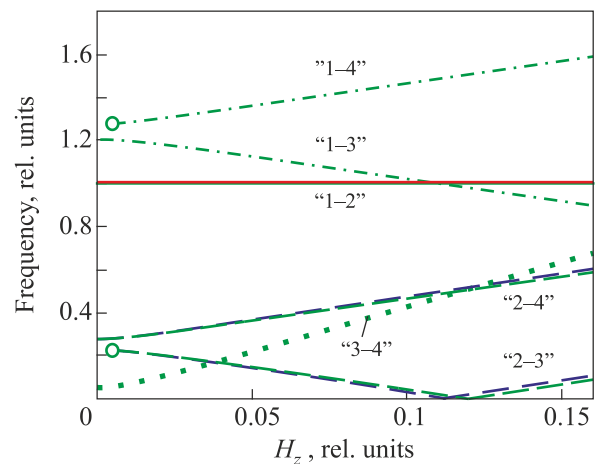


Fig. 6. (Color online) EPR spectra in a magnetic field $\mathbf{H} \parallel \mathbf{z}$, $\phi_1 = 0, \psi_1 = 0$. Transition designations correspond to Fig. 1. Color coding: $\theta_1 = 0$ (blue), $\pi/4$ (green), $\pi/2$ (red). Critical fields, where EPR line disappears, are marked with open circles. Two overlapping horizontal lines present transitions “1–2” for $\theta_1 = \pi/4$ and $\pi/2$.

Determination of the deflection of the LCS axes about the angle ψ_1 is due to the choice of the $\mathbf{x}^{(k)}$ -axis direction, which, in contrast to the ligand orientation of $\mathbf{z}^{(k)}$, has a less transparent physical meaning. In addition, as shown in Sec. 3, the states $|0,0\rangle_{UCS}$ and $|1,0\rangle_{UCS}$ do not change when LCS rotate about the angle ψ_1 , while the states $|1,1\rangle'_{UCS}$ and $|1,1\rangle''_{UCS}$ are mutually equivalent for $\psi_1 = 0$ and $\psi_1 = \pi/2$. At $\psi_1 = \pi/4$, $|1,1\rangle'_{UCS}$ and $|1,1\rangle''_{UCS}$ coincide and are average of $\psi_1 = 0$ and $\psi_1 = \pi/2$ cases. Therefore, other fundamentally different field dependences should not be expected for the EPR spectra for $\psi_1 = \pi/4$ and $\psi_1 = \pi/2$, than for $\psi_1 = 0$, and these cases are not considered in this paper.

5. Conclusion

A strong crystal field that holds the local axes of paramagnetic ions commonly in different directions completely destroys the magnetic system of the $s = 1/2$ dimer in the UCS representation. The arrangement of the antisymmetric and symmetric wave functions with $S_z = 0$ is opposite concerning to the system with UCS and is a consequence of the C_2 symmetry only.

The rotation symmetry of the two-spin $s = 1/2$ system with the LCS axes being subject to the symmetry operation C_2^1 reflects the C_2 symmetry for all spin states (Fig. 2). This result is not obvious for a spin $1/2$ system that generally is not subject to the $SO(3)$ symmetry.

Let us discuss the effect of misorientation of the LCS ion axes with a change only in the angle ϕ_1 with nonzero θ_1 . For the dependences $\langle S_z^2(\theta_1) \rangle$ of the state $|0,0\rangle_{UCS}$, this difference is quite significant and looks like the appearance of a nonzero spin of this level. In terms of the mutual orientation of LCS, the cases $\phi_1 = 0$ and, for example, $\phi_1 = \pi/2$ (Fig. 2) differ in that initially the $\tilde{\mathbf{x}}^{(k)}$ axes are antiparallel for collinear $\tilde{\mathbf{z}}^{(k)}$, and for $\phi_1 = \pi/2$, $\tilde{\mathbf{x}}^{(k)}$ are collinear for antiparallel $\tilde{\mathbf{z}}^{(k)}$. The effect of an increase in ϕ_1 at $\theta_1 \neq 0$ on the spin components consists in the transfer of the s_x and/or s_y components of the $s^{(1)}$ and $s^{(2)}$ spins to the S_z component of the “molecular” spin. In terms of spin correlations, this means the magnetic properties can be provided s_x-s_x and/or s_y-s_y correlations even if the magnetic system loses the s_z-s_z correlations.

It should be noted that the maximum number of lines in the spectrum of the spin dimer (5–6) is in the range of $\theta_1 \sim \pi/4$, while the width of this region strongly depends on the angles ϕ_1 and ψ_1 . There is either one line or, if $\phi_1 = \pi/2$, none observed near $\theta_1 \cong \pi/2$ (“silent” EPR mode). Let us compare the behavior of the intensity of EPR transitions and average square spin values if $\phi_1 = 0$ and $\psi_1 = 0$ [Fig. 2(a), Fig. 3]. Mixing of spin states with an increase in θ_1 will unblock “forbidden” transitions and lead to the appearance of transitions “1–2”, “1–3” and “3–4”. In $\theta_1 \cong \pi/2$, these transitions, as well as “2–4”, disappear, and no EPR is observed (“silent” EPR mode). Given the latter, we can suggest the correlation between the spin states of the dimer at zero azimuthal angles of deflection of the LCS

and the intensity of the EPR lines. If $\phi_1 \neq 0$ and/or $\psi_1 \neq 0$, the qualitative coincidence of the evolution of spin states and the intensity of EPR lines is observed just for some of transitions and requires further study.

So far, the work has considered the effect of only one operation, C_2^1 on the spin system, which can exist only with the approximate molecular symmetry C_2 . Let us consider briefly the effect of other symmetry operations.

The unit matrices $+\mathbf{I}$, $-\mathbf{I}$ or the same matrices with imaginary units in the diagonal determine the inversion operation. The transformation result in all four cases — $O \mathbf{s}^{(k)} O'$, where O is the inversion, strictly equivalent to the identical transformation E . That is, the SMM with inversion only is equivalent to a spin system with UCS. The plane of symmetry passing through the middle of the bond $s^{(1)}-s^{(2)}$ ($\perp \mathbf{x}$) can be represented as a rotation around the x axis about an angle π and subsequent inversion. Since the inversion permutes the spins in this case, we again obtain an UCS-equivalent system. Operations that do not permute $s^{(1)}$ and $s^{(2)}$ cannot impose any constraints on interactions in the spin system and do not matter in this case. Thus, C_2^1 with the axis perpendicular to the $s^{(1)}-s^{(2)}$ link is the only symmetry operation that imposes symmetry constraints on the $s = 1/2$ dimer.

The question arises: how often do $s = 1/2$ dimers with approximate symmetry C_2 occur? Despite the many known spin-1/2 binuclear clusters [6–40], one V^{4+} and one Cu^{2+} compounds are given in the Introduction. The overwhelming majority of Cu^{2+} compounds have only an inversion center, several of them have a symmetry plane perpendicular to the $s^{(1)}-s^{(2)}$ bond. They both refer to dimers with UCS, i.e., are adequately described by the traditional Hamiltonian. In addition, at small deflection angles θ_1 of the axes, the differences between the energy spectrum and the spin states of the dimer (Fig. 2) and the case with UCS are extremely small. Based on the foregoing, we may suggest a very rare opportunity to observe manifestations of C_2 symmetry in experimental studies of spin dimers. Such observations require high-quality single-crystal EPR studies in the frequency range up to $\sim (J+A_{ax}+A_{rh})$. An additional indicator able to detect the effects of LCS noncollinearity in a $1/2$ spin system is an anomalous spectroscopic splitting factor (g) as an indicator of a strong crystal field with mismatched local axes.

The symmetry analysis model for noncollinear local spin-coordinate systems, first presented in this paper, limits the range of objects suitable for study by molecular symmetry, which allows for a permutation axis C_2 in the absence of inversion symmetry. Although the model is used here only for $s = 1/2$ dimers, it can be also applied to study other small spin clusters.

1. R. Sessoli, D. Gatteschi, A. Caneschi, and M. A. Novak, *Nature (London)* **365**, 141 (1993).
2. D. Gatteschi and L. Pardi, *Gazzetta Chim. Ital.* **123**, 231 (1993).

3. D. V. Efremov and R. A. Klemm, *Phys. Rev. B* **74**, 064408 (2006).
4. O. Waldmann, *Phys. Rev. B* **61**, 6138 (2000).
5. W. Florek and S. Bucikiewicz, *Phys. Rev. B* **66**, 024411 (2002).
6. G. Kamieniarz, R. Matysiak, A. Caramico D'Auria, F. Esposito, and C. Benelli, *Eur. Phys. J. B* **23**, 183 (2001).
7. I. S. Camara, R. Gautier, E. Le Fur, J.-C. Trombe, J. Galy, A. M. Ghorayeb, and A. Stepanov, *Phys. Rev. B* **81**, 184433 (2010).
8. G. M. Larin, V. V. Minin, and V. F. Shulgin, *Russian Chem. Rev.* **77**, 451 (2008).
9. R. P. Sartoris, V. T. Santana, E. Freire, R. F. Baggio, O. R. Nascimento, and R. Calvo, *Dalton Trans.* **49**, 5228 (2020).
10. S. S. Massoud, M. Spell, C. C. Ledet, T. Junk, R. Herchel, R. C. Fischer, Z. Trávníček, and F. A. Mautner, *Dalton Trans.* **44**, 2110 (2015).
11. S. Jana, B. K. Shaw, P. Bhowmik, K. Harms, M. G. B. Drew, S. Chattopadhyay, and S. K. Saha, *Inorg. Chem.* **53**, 8723 (2014).
12. L. Rigamonti, A. Cinti, A. Forni, A. Pasini, and O. Piovesana, *Eur. J. Inorg. Chem.* **2008**, 3633 (2008).
13. L. Rigamonti, A. Forni, R. Pievo, J. Reedijk, and A. Pasini, *Inorg. Chim. Acta* **387**, 373 (2012).
14. I. Fernández, R. Ruiz, J. Faus, M. Julve, F. Lloret, J. Cano, X. Ottenwaelder, Y. Journaux, and M. C. Muñoz, *Angew. Chem.* **113**, 3129 (2001).
15. I. Castro, M. L. Calatayud, J. Sletten, F. Lloret, J. Cano, M. Julve, G. Seitz, and K. Mann, *Inorg. Chem.* **38**, 4680 (1999).
16. J. P. Naskar, C. Biswas, B. Guhathakurta, N. Aliaga-Alcalde, L. Lu, and M. Zhu, *Polyhedron* **30**, 2310 (2011).
17. A. K. Singh, J. I. van der Vlugt, S. Demeshko, S. Dechert, and F. Meyer, *Eur. J. Inorg. Chem.* **2009**, 3431 (2009).
18. F. Z. Chiboub Fellah, J.-P. Costes, L. Vendier, C. Duhayon, S. Ladeira, and J.-P. Tuchagues, *Eur. J. Inorg. Chem.* **2012**, 5729 (2012).
19. C. G. Efthymiou, C. P. Raptopoulou, V. Psycharis, A. J. Tasiopoulos, A. Escuer, S. P. Perlepes, and C. Papatriantafyllopoulou, *Polyhedron* **64**, 30 (2013).
20. S. Triki, C. J. Gómez-García, E. Ruiz, and J. Sala-Pala, *Inorg. Chem.* **44**, 5501 (2005).
21. S. Adhikari, A. Banerjee, S. Nandi, M. Fondo, J. Sanmartin-Matalobos, and D. Das, *RSC Adv.* **5**, 10987 (2015).
22. A. Ray, G. M. Rosair, G. Pilet, B. Dede, C. J. Gómez-García, S. Signorella, S. Bellú, and S. Mitra, *Inorg. Chim. Acta* **375**, 20 (2011).
23. J. Carranza, J. Sletten, F. Lloret, and M. Julve, *Preparation, crystal structure and magnetic properties of di-2-pyridylamine (dpa) copper(II) complexes [Cu(dpa)(N₃)₂]_n and [Cu₂(dpa)₂(NCO)₄]*, *J. Molec. Struct.* **890**, 31 (2008).
24. P. Gómez-Saiz, R. Gil-García, M. A. Maestro, F. J. Arnaiz, L. Lezama, T. Rojo, J. L. Pizarro, M. I. Arriortúa, M. González-Álvarez, J. Borrás, V. Diez-Gómez, and J. García-Tojal, *Eur. J. Inorg. Chem.* **2009**, 373 (2009).
25. J. Casanova, G. Alzuet, J. Latorre, and J. Borrás, *Inorg. Chem.* **36**, 2052 (1997).
26. E. Aznar, S. Ferrer, J. Borrás, F. Lloret, M. Liu-González, H. Rodríguez-Prieto, and S. García-Granda, *Eur. J. Inorg. Chem.* **2006**, 5115 (2006).
27. Soma Sen, *International Journal of Engineering, Science and Mathematics* **7**(4), 154 (2018).
28. P. Bhunia, D. Banerjee, P. Datta, P. Raghavaiah, A. M. Z. Slawin, J. D. Woollins, J. Ribas, and C. Sinha, *Eur. J. Inorg. Chem.* **2010**, 311 (2010).
29. A. M. Madalan, M. Noltemeyer, M. Neculai, H. W. Roesky, M. Schmidtman, A. Müller, Y. Journaux, and M. Andruh, *Inorg. Chim. Acta* **359**, 459 (2006).
30. C. Aronica, E. Jeanneau, H. E. Moll, D. Luneau, B. Gillon, A. Goujon, A. Cousson, M. A. Carvajal, and V. Robert, *Chem. Eur. J.* **13**, 3666 (2007).
31. W. A. Alves, A. C. Sant'Ana, M. P. Abbott, P. Homem-de-Mello, H. Martinho, R. H. A. Santos, J. G. Ferreira, M. L. A. Temperini, A. Paduan-Filho, and A. M. da Costa Ferreira, *Sci. Adv. Mater.* **2**, 1 (2010).
32. J.-K. Tang, Y. Ou-Yang, H.-B. Zhou, Y.-Z. Li, D.-Z. Liao, Z.-H. Jiang, S.-P. Yan, and P. Cheng, *Crystal Growth & Design* **5**, 813 (2005).
33. A. Prokofieva, A. I. Prikhod'ko, E. A. Enyedy, E. Farkas, W. Maringgele, S. Demeshko, S. Dechert, and F. Meyer, *Inorg. Chem.* **46**, 4298 (2007).
34. S. C. Manna, J. Ribas, E. Zangrando, and N. R. Chaudhuri, *Inorg. Chim. Acta* **360**, 2589 (2007).
35. K. B. Szpakolski, K. Latham, C. J. Rix, and J. M. White, *Eur. J. Inorg. Chem.* **2010**, 5660 (2010).
36. M. J. Belousoff, B. Graham, B. Moubaraki, K. S. Murray, and L. Spiccia, *Eur. J. Inorg. Chem.* **2006**, 4872 (2006).
37. S. Saha, S. Koner, J.-P. Tuchagues, A. K. Boudalis, K.-I. Okamoto, S. Banerjee, and D. Mal, *Inorg. Chem.* **44**, 6379 (2005).
38. B. Sreenivasulu, F. Zhao, S. Gao, and J. J. Vittal, *Eur. J. Inorg. Chem.* **2006**, 2656 (2006).
39. N. Lah, I. Leban, and R. Clérac, *Eur. J. Inorg. Chem.* **2006**, 4888 (2006).
40. I. Monte-Pérez, A. M. Sosa, S. Bernès, N. Aliaga-Alcalde, V. M. Ugalde-Saldívar, and L. Gasque, *Eur. J. Inorg. Chem.* **2012**, 4739 (2012).

Двоядерний $s = 1/2$ мономолекулярний магнетик
з симетрійними обмеженнями

A. V. Zhuravlev

Досліджено вплив обмінної анізотропії на мономолекулярний магнетик з тотожними $s^{(1)} = s^{(2)}$ спінами, підпорядкованими C_2 групі симетрії. Гамільтоніан в поданні двоспінових 4×4 матриць Паулі в локальних системах координат, що є неколінеарними, перетворено

до подання загальної системи координат і використано для визначення рівнів енергії та спінових станів. Виявлено аномальну еволюцію усереднених спінів магнітної системи при відхиленні локальних осей анізотропії. Передбачено повністю немагнітний стан $s = 1/2$ спінового димера, а також «німу» моду ЕПР. Визначено кутові межі існування ЕПР для будь-яких можливих вза-

ємних відхилень локальних осей іонів для кожного з 6 можливих переходів між рівнями спінової системи, як в нульовому, так і в кінцевому магнітному полі.

Ключові слова: молекулярний магнетизм, обмінні взаємодії (електронні), магнітна анізотропія, спіновий кросовер, ЕПР спектроскопія.